JACS
JOURNAL OF THE AMERICAN CHEMICAL SOCIETY
Article
pubs.acs.org/JACS

A Biradical Balancing Act: Redox Amphoterism in a Diindenoanthracene Derivative Results from Quinoidal Acceptor and Aromatic Donor Motifs

Gabriel E. Rudebusch,[†] Guzmán L. Espejo,[‡] José L. Zafra,[‡] Miriam Peña-Alvarez,[‡] Sarah N. Spisak,[§] Kotaro Fukuda,[∥] Zheng Wei,[§] Masayoshi Nakano,*[,∥] Marina A. Petrukhina,*[,§] Juan Casado,*[,‡] and Michael M. Haley*[,†]

[†]Department of Chemistry & Biochemistry and the Materials Science Institute, University of Oregon, Eugene, Oregon 97403-1253, United States

[‡]Department of Physical Chemistry, University of Málaga, Campus de Teatinos s/n 2, 29071 Málaga, Spain

[§]Department of Chemistry, University at Albany, State University of New York, Albany, New York 12222-0100, United States

[∥]Department of Materials Engineering Science, Graduate School of Engineering Science, Osaka University, Toyonaka, Osaka 560-8531, Japan

Supporting Information

ABSTRACT: The reduced and oxidized states of an open-shell diindeno[*b*,*i*]anthracene (**DIAn**) derivative have been investigated by experimental and theoretical techniques. As a result of moderate biradical character and the ability of cyclopenta-fused scaffolds to stabilize both positive and negative charges, **DIAn** exhibits rich redox chemistry with four observable and isolable charged states. Structural and electronic properties of the **DIAn** system are brought to light by UV−vis−NIR and Raman spectroelectrochemical measurements. Aromatization of the diindeno-fused anthracene core upon successive single-electron injections is revealed through single-crystal X-ray diffraction of radical anion and dianion salts. We present a rare case where the pseudoaromatic/quinoidal ground state of a neutral biradical polycyclic hydrocarbon leads to a stable cascade of five redox states. Our detailed investigation of the transformation of molecular structure along all four redox events provides a clearer understanding of the nature of charge carriers in ambipolar organic field-effect transistors.

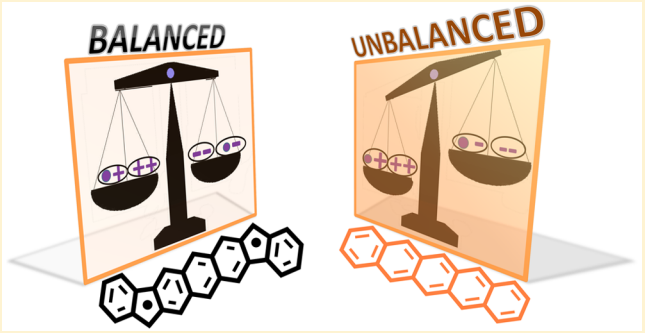

INTRODUCTION

Polycyclic hydrocarbons (PCHs) very often exhibit rich redox chemistry in addition to unique electronic and optical properties. Explorations of the charge distribution, magnetism, electronic structure, and solid-state morphology of redox-active PCHs are well-engrained areas of physical organic chemistry.[1−5] The practical application of redox-active PCHs and related materials has seen considerable growth in recent years as the limits of traditional inorganic-based systems are becoming evident.[6−8] A related field experiencing a burst of activity involves the synthesis and characterization of PCHs with biradical character.[9−12] Typically, high levels of reactivity are associated with the pair of loosely correlated electrons. As a consequence of new synthetic approaches and improved spectroscopic techniques, numerous stable biradical PCHs have been reported in the past decade.[10,11] The molecules exhibit many favorable properties, including redox amphoterism, strong absorption in the visible spectrum, small frontier orbital energy gaps (<1.5 eV), large second hyperpolarizabilities, and the opportunity of modulating spin state through thermally accessible triplet states.[13−15]

Generally, most of these π-conjugated systems are excellent electron donors, easily stabilizing positive charges, and, proportionally, only a few are good electron acceptors able to stabilize negative charges. This originates from the abundance of p-type semiconductors (e.g., acenes, oligothiophenes)[16] and the recent increase of n-type semiconductors (e.g., rylene diimides, fullerene-based acceptors).[17] In this context, ambipolar semiconductors represent "water in the desert" given the inherent difficulty of the same π−conjugated structure to equally accommodate charge carriers of either sign.[18,19] The connection between ambipolar semiconductor behavior and molecular redox amphoterism is well-established, and this has been discovered in PCHs with moderate biradical character.[10] The electronic configuration of a biradical PCH is described by the relatively high-lying highest occupied molecular orbital (HOMO) energy and low-lying lowest unoccupied molecular orbital (LUMO) energy, which, in concert, provides the

Received: July 29, 2016
Published: August 30, 2016

DOI: 10.1021/jacs.6b07882
J. Am. Chem. Soc. 2016, 138, 12648−12654

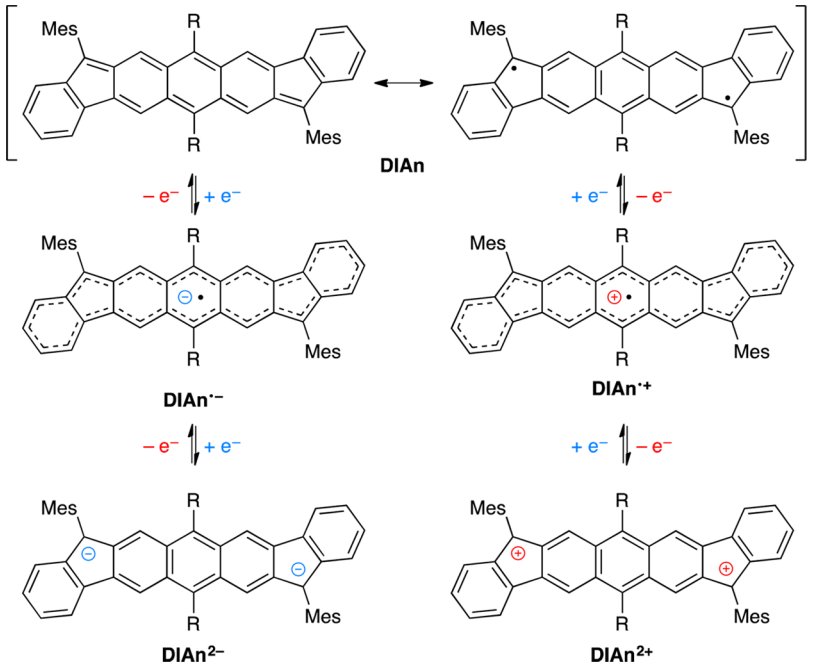

Figure 1. Redox processes of **DIAn**. The ground state is a resonance hybrid of quinoidal (acceptor, top left) and aromatic (donor, top right) structures. R = (triisopropylsilyl)ethynyl.

thermodynamic driving force for reversible injection and extraction of electrons.

The application of redox-active biradical PCHs is only recently coming into the fold of organic electronics and spintronics. Organic radical batteries based on stable nitroxyl radical polymers[20] or trioxotriangulene systems[21] are attractive alternatives to the current generation of metal ion batteries given their fast charging speed, cycling stability, and environmental sustainability. Information storage using redox-active organic compounds as memory elements is another potentially fruitful area of research as a single molecule could, in principle, represent the physically smallest bit of information.[22] The prospects of controlling molecular spin information by varying redox states is an appealing aspect of redox responsive PCHs. A remarkable example of a viologen-containing homocatenane with six accessible and air-stable charged states was recently reported.[23] The interlocked molecule was shown to switch between diamagnetic and paramagnetic forms as a function of oxidation state. The ability to stabilize both negative and positive charges, as well as metal-like electron delocalization in the solid state, has been exploited in ambipolar organic field-effect transistors (OFETs) based on redox amphoteric small molecules.[24,25] Koike and co-authors demonstrated highly coherent band transport in thin films based on an indacenodiphenalene derivative. The excellent performance of the OFETs is likely due to the intimate $\pi-\pi$ contacts and multi-center bonding between molecules.[26]

We recently reported the diindeno[*b*,*i*]anthracene derivative **DIAn** as an oxygen- and temperature-stable singlet biradical compound (Figure 1).[27] The ground-state is best described as a balance of quinoidal closed-shell and aromatic open-shell resonance structures. In connection with a frontier orbital energy gap of 1.45 eV and a moderate biradical character index[28] of $y = 0.62$, **DIAn** exhibits two reversible one-electron reductions and two reversible one-electron oxidations, as disclosed in the cyclic voltammetry (CV) experiment (Figure 2).[27] The marked symmetry between all four redox waves, indicating

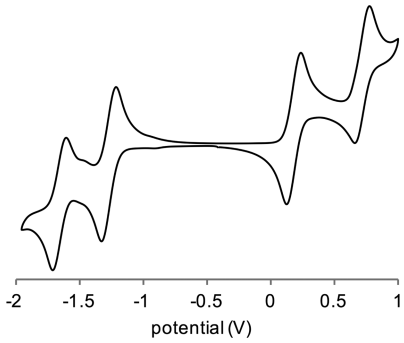

Figure 2. Cyclic voltammogram of **DIAn** in CH_2Cl_2 vs ferrocene/ferrocenium.

similar electro-kinetic parameters and good resolution between waves (ΔE_{red} = 0.39 V, ΔE_{ox} = 0.53 V), led to the hypothesis that each charged species in Figure 1 could be accessed and characterized independently. Indeed, the stability and efficient gram-scale synthesis of **DIAn** facilitate further experiments and exploration of this new open-shell PCH scaffold. While redox-active biradical PCHs based on large acene cores are known,[29−31] this study represents a thorough experimental and theoretical investigation of the reduced and oxidized states of **DIAn** and the transformation of molecular structure along all four redox events. Our results provide a clearer understanding of the nature of charge carriers in ambipolar OFETs and serve as a platform for further modification of the diindenoacene family.[24,27,32−37]

RESULTS AND DISCUSSION

UV−Vis−NIR Absorption Spectroelectrochemistry. The redox processes examined in solution cyclic voltammetry were studied by UV−vis−NIR spectroelectrochemistry. In the anodic branch (Figure 3, top), the first one-electron oxidation gives rise to a spectrum with two main bands at 867 and 1945 nm. Interestingly, a peak at 867 nm is also observed when **DIAn** is

DOI: 10.1021/jacs.6b07882
J. Am. Chem. Soc. 2016, 138, 12648−12654

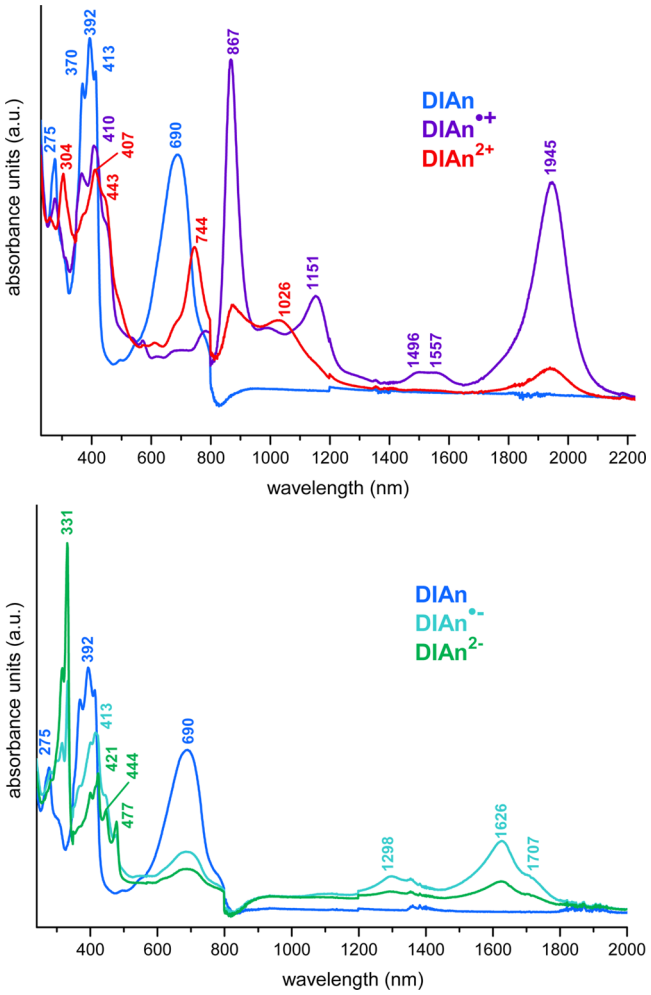

Figure 3. Oxidation (top) and reduction (bottom) of **DIAn** followed by UV−vis−NIR spectroelectrochemistry. Conditions: CH_2Cl_2, 0.1 M $[n\text{-}Bu_4N][PF_6]$.

heated to 135 °C in 1,1,2,2-tetrachloroethane (Supporting Information, Figure S1) with the intensity showing a decrease upon cooling to 25 °C. This could be due to a reversible redox process with oxygen. Nonetheless, the reversibility of the reaction reveals the robustness of the material versus degradative oxidation. The low-energy absorbance (1945 nm, 0.65 eV) is typical of a PCH radical cation and can be assigned to a singly occupied molecular orbital (SOMO) → LUMO transition,[38] while the 867 nm absorbance has major contributions from the HOMO → SOMO transition of **DIAn**$^{\bullet+}$ (Figure S25). Increasing the anodic potential further yields two new bands centered at 744 and 1026 nm, presumably due to **DIAn**$^{2+}$. The low-energy absorption can be assigned to a weak HOMO → LUMO transition (Figure S26).

The one-electron reduction process shows disappearance of the neutral absorption at 690 nm and the emergence of two groups of bands centered at 1600−1700 nm and at 400 nm (Figure 3, bottom). The low-energy absorbance (~0.75 eV) can be attributed to a HOMO → SOMO single transition of **DIAn**$^{\bullet-}$ (Figure S23). Again, this is typical of a quinoidal PCH radical anion where the skeletal backbone has regained partial aromaticity.[39,40] With increasing cathodic potential, a clear progression to **DIAn**$^{2-}$ is observed, with new peaks at 330 nm and typical rigid acene absorbance from 440 to 470 nm. These anthracene-like vibronic features are in good agreement with those of the dihydro precursor of **DIAn** that also contains an aromatic anthracene core appended by saturated indeno fragments (Figure S4).[27] According to the optimized structures for model **DIAn**$^{\bullet+}$ and **DIAn**$^{\bullet-}$ redox species, one would expect further likeness between their absorption spectra, which only differ by 0.1 eV for the low-energy bands. This slight energy difference indicates the comparable charge delocalization either of a hole among many π-electrons (i.e., $n-1$ electrons with n the number in the neutral state) or of an electron in a similar electron cloud (i.e., with n electrons). A comparable effect is more significant in the **DIAn**$^{2-}$/**DIAn**$^{2+}$ pair due the increasing number of holes/electrons. In parallel with the spectroelectrochemical experiment, chemical reduction with K metal and oxidation with $NOBF_4$ gave analogous absorption spectra (Figures S2 and S3), thus confirming the assignment of the UV−vis−NIR electrolysis experiments.

Vibrational Raman Spectroelectrochemistry. Raman spectroelectrochemical measurements were carried out to investigate the change in molecular structure with each redox event. The Raman spectra of **DIAn** during electrolysis are shown in Figure 4a. We focus our analysis to the 1600−1550 cm^{-1} spectral range where the structurally relevant C=C stretching vibrations of PCH backbones, ν(C=C), appear. The Raman spectrum of neutral **DIAn** shows a band at 1590 cm^{-1} due to the characteristic ν(C=C) stretching mode of the pseudoaromatic biradical anthracene structure. One electron oxidation produces **DIAn**$^{\bullet+}$ with a pair of bands at 1587 and 1581 cm^{-1}. Interestingly, the Raman spectrum upon one-electron reduction to **DIAn**$^{\bullet-}$ is also characterized by a band at 1580 cm^{-1}. After the second one-electron oxidation to **DIAn**$^{2+}$, the spectrum is simplified to a single band at 1580 cm^{-1}. In the cathodic branch, a second one-electron reduction to **DIAn**$^{2-}$ again yields a similar Raman spectrum with a single band at 1582 cm^{-1}. What is significant among the different spectra is that either redox process results in Raman dispersions with main skeletal ν(C=C) bands appearing within a small range of frequencies; there is large vibrational spectroscopic resemblance revealing the structural similarities between the doubly charged species independent of sign. This evidence suggests that the ground electronic delocalization of holes/electrons in the redox species is similar in anion/cation and dianion/dication couples in analogy with the relationship found in the UV−vis−NIR absorption spectra.

We have previously assigned the 1580 cm^{-1} band as the characteristic feature of the triplet excited state of neutral **DIAn** resulting from the gain of aromatic character in this thermally accessible high spin state.[27] Therefore, the appearance of ν(C=C) bands in the charged species near 1580 cm^{-1} is an indicator of the recovery of aromaticity in the **DIAn** core. It can be inferred that the accumulation of aromatic character during redox events is the most efficient mode of stabilizing charges of both sign. From a structural viewpoint, this can be an explanation for the mirror-like reduction and oxidation events in the CV experiment. Further, the ability to stabilize both radical anions and cations has implications in describing the microscopic charge carriers and ambipolar charge transport properties previously shown in OFETs fabricated from **DIAn**.[27]

This ability of the neutral biradical **DIAn** to access this "aromatic transformation" under different stimuli (redox, heating, etc.) was also explored under mechanical stress by applying high pressure to the solid at room temperature (Figures S11−S15 and Table S2). The variable-pressure experiment was followed by Raman spectroscopy, and the results are shown in Figure 4b,c. The main Raman band under 532 nm laser excitation appears at

DOI: 10.1021/jacs.6b07882
J. Am. Chem. Soc. 2016, 138, 12648−12654

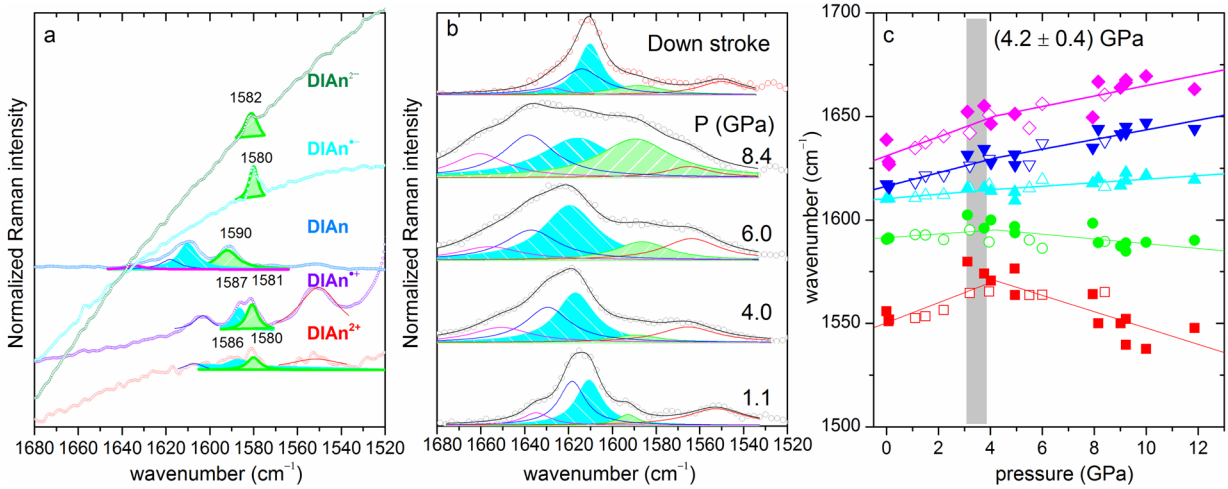

Figure 4. (a) Raman spectroelectrochemical experiment of **DIAn** excited at 785 nm. Neutral spectrum is taken at 633 nm. Conditions: 10^{-1} M with 0.1 M [*n*-Bu_4N][PF_6] in CH_2Cl_2. (b) Raman spectrum at selected pressures measured with a laser of 532 nm in the 1680−1520 cm^{-1} region. The spectra have been fitted to five contributions, which at room conditions are at: 1630, 1615, 1610, 1580, and 1550 cm^{-1}, in red, dark blue, filled cyan, filled green, and filled red, respectively. Under ambient conditions the 1615−1610 cm^{-1} contributions are the most intense, corresponding to ν(C═C) of the quinoidal resonance hybrid. The 1580 cm^{-1} band that gains intensity with increasing pressure corresponds to the ν(C═C) of an anthracene-like core in **DIAn**. (c) Raman shift pressure evolution of the fitted contributions from experimental Raman spectra taken with 633 and 532 nm, filled and empty symbols, respectively. Each color corresponds to the fitted contribution. Vertical gray region corresponds to the inflection point in the linear trend.

1615 cm^{-1} with a shoulder at 1610 cm^{-1} and a set of weak bands 1630, 1580, and 1550 cm^{-1}. Under external pressure of 8.4 GPa, the set of weak bands are intensified with respect to the strongest band at normal pressure; however, within these new bands there is an accentuation of the 1581 cm^{-1} feature that reaches the intensity of the 1610 cm^{-1} band (see deconvoluted spectra in Figure 4b). As shown in Figures S11 and S13, there are additional peaks in the 1200−1300 cm^{-1} spectral region that are also altered by pressure, as revealed by their relative intensities at room and high applied pressure. The distinct response of the 1650−1550 cm^{-1} molecular vibration bands to pressure (see Figure 4c) and the fact that the low-wavenumber crystal−phonon Raman region scarcely changes in the experiment (the unit cell structure is thus unchanged in the experiment) are arguments in support of the induction of molecular-level changes upon applied pressure. In the ν(C═C) frequency region, again, the 1580 cm^{-1} band has a major presence, which, according to the assignment above, should arise from a gain in anthracene-like aromatic character in the **DIAn** core. We can speculate that, under high pressure, (i) the cofacial π−π arrangement of the **DIAn** molecules allows self-exchange of electrons, giving rise to a kind of charge-transfer complex; (ii) since the molecules are forced closer at high pressure, and given the slipped 1D packing in the solid state, the formation of strained long C−C bonds between radicals between neighboring molecules might induce the formation of aromatic moieties; and (iii) sample heating due to adiabatic compression should be ruled out as a source of increased triplet population, given that the singlet−triplet gap could be simultaneously increased due to enhanced intermolecular interactions. Taken together, the results of the variable-pressure experiment highlight the structural changes of the biradical **DIAn** system in response to molecular compression.

Solid-State Structures of Reduced DIAn Species. To gain insight into the structural changes upon one and two electron reductions, we sought to prepare and characterize salts of the radical anion and dianion of **DIAn** in the solid state.[41] Brief exposure of the deep violet THF solution of **DIAn** to K metal in the presence of 18-crown-6 ether provided the solvent-separated radical anion salt **1** (Scheme 1) that crystallized as dark brown plates. An X-ray diffraction study showed the **DIAn**$^{\bullet-}$ anion is centrosymmetric and planar; root-mean-squared (RMS) deviation through an average plane drawn through the core is calculated to be 0.05 Å. Longer exposure to K metal provided the dianion **2** crystallized from THF/hexanes as red-brown plates. The **DIAn**$^{2-}$ core was found to be centrosymmetric and planar with a RMS deviation of 0.09 Å. Interestingly, the outer benzenoid rings are canted ca. 10° from the central anthracene ring toward the K^+ ion. Using similar experimental conditions, but with diglyme in place of 18-crown-6 ether, the contact-ion pair product **3** was crystallized from the reaction as orange-brown plates. The [K(diglyme)(THF)]$^+$ ions are disordered over two positions with short K···π-contacts of 2.91 Å (η^5) and longer ones of 3.26 (η^6) (Figure S9). In **3**, the **DIAn**$^{2-}$ core is severely distorted from planarity. Notably, **1** and **2** lack metal ion−π interactions; the [K(18-crown-6)$(THF)_2$]$^+$ cations are located 5.67 Å (**1**) and 6.24 Å (**2**) from the polycyclic core. This permits meaningful comparison of bond distances between the neutral ligand and "naked" reduced species.[42] Analysis of the bond distances of the non-contact ion pair products **1** and **2** reveals aromatization of the anthracene core (Figure 5). In the first reduction event, bonds b, d, f, h, and i show an average contraction of 0.017 Å. These bonds were previously ascribed partial single bond character in neutral **DIAn**. Double bonds c, e, and g throughout the core remain unaffected. The structure of **1** preserves the bond distance alternation of the neutral ligand, but, as a result of an electron in a previously non-bonding orbital, there is contraction of bond distances in the core.[35,43] The [K(18-crown-6)$(THF)_2$]$^+$ ion is slipped by just 1.21 Å from the **DIAn**$^{\bullet-}$ centroid, indicating full delocalization of the free electron (Figure 1). The next single-electron reduction to give dianion **2** shows the homogenization of central bonds d, e, f, and g to 1.420(±0.005) Å, a value indicative of an anthracene-like structure. In fact, comparison of the bond

DOI: 10.1021/jacs.6b07882
J. Am. Chem. Soc. 2016, 138, 12648−12654

Scheme 1. Synthesis of Radical Anion (1) and Dianion Salts (2, 3) of DIAn by Potassium-Induced Reduction[a,b]

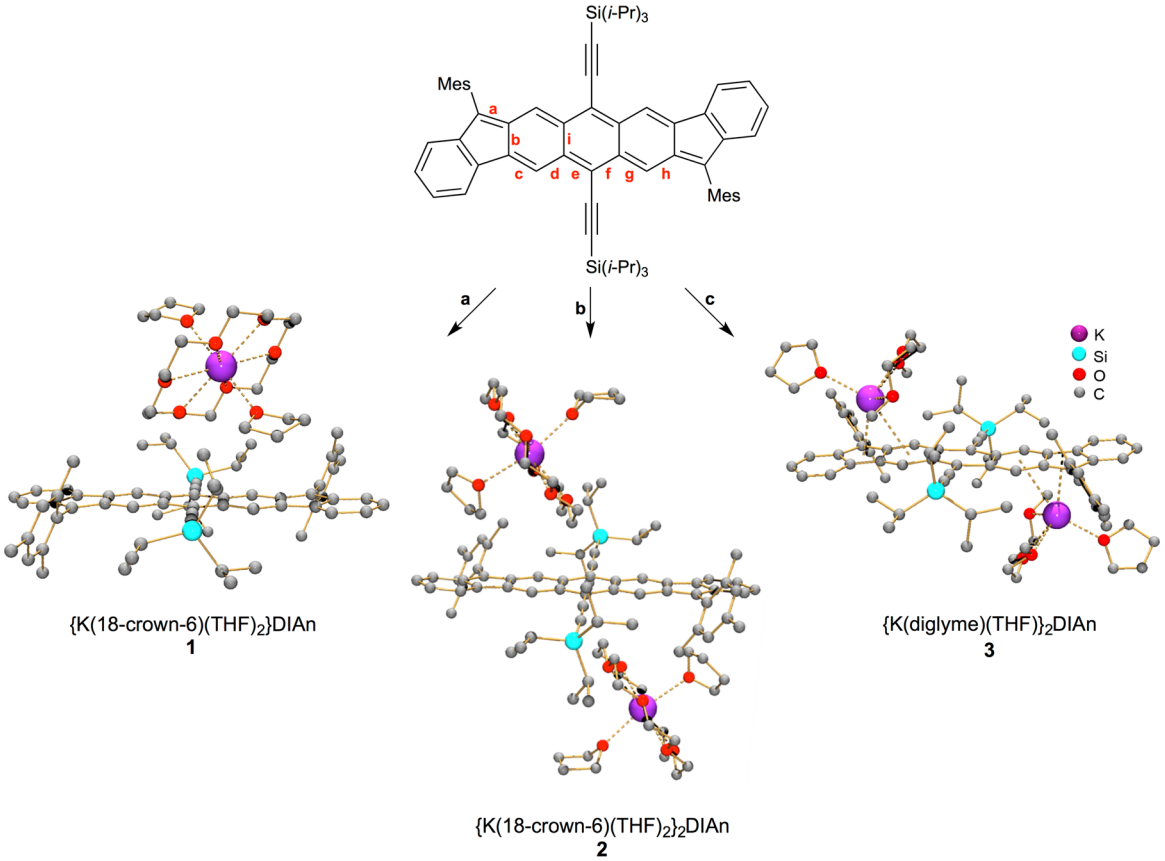

[a]Reaction conditions: (a) K, 18-crown-6, THF, 10 min; (b) K, 18-crown-6, THF, 2 h; (c) K, THF, 10 h, then diglyme/hexanes layering. [b]All H-atoms in the ball-and-stick X-ray structure models of **1**−**3** omitted for clarity.

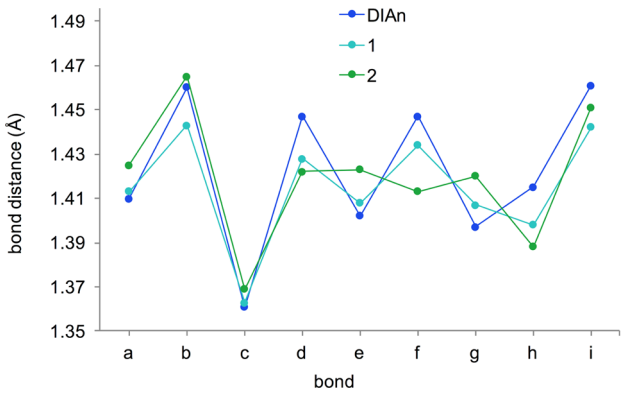

Figure 5. Single-crystal X-ray diffraction studies of neutral **DIAn** (blue), radical anion (**1**, teal), and dianion (**2**, green), disclosing aromatization of the core upon reduction. See bond lettering in Scheme 1.

length in **2** to the structural data of a similar saturated system gives excellent agreement (Figure S10). From the solid-state structure of **1** we observe that the first reduction results in contracted bond distances but overall retention of the quinoidal bonding pattern. The second reduction toward **2** completes the aromatization of the anthracene core. Considering the η^5-coordination of K in the contact-ion pair **3**, we can infer that the negative charges are predominantly localized on the five-membered rings giving two cyclopentadienyl-like anions that straddle the central anthracene (Figure 1).

Computational Assessment. Quantum chemical calculations were carried out to further scrutinize the neutral, reduced, and oxidized states of **DIAn**. For computational ease, the Si(*i*-Pr)$_3$ and mesityl groups in **DIAn** were simplified to SiMe$_3$ and 2,6-dimethylphenyl, respectively. Geometry optimization of the neutral state is carried out using the RB3LYP/6-311G* method, which has been confirmed to well reproduce the X-ray crystallographic data and the simplified optimized geometry at a higher level of theory, the spin-flip TD-DFT method.[27] On the other hand, for the geometry optimization of the singly reduced and oxidized states, the UB3LYP/6-311G* level of theory was chosen since it has been previously confirmed to well reproduce the geometries and excitation energies for charged PCHs.[44] Since the doubly reduced and oxidized states do not give open-shell solution, we adopted the RB3LYP/6-311G* method. The optimized geometry of the reduced model **DIAn** and the experimentally derived solid-state structures of **1** and **2** are in excellent agreement (Supporting Information).

Compared with the neutral state, the singly reduced and oxidized states similarly exhibit smaller bond-length alternation at the core anthracene moiety, while the doubly reduced and oxidized states exhibit even more diminished bond-length alternation. These computational results also support the resonance structures drawn in Figure 1 and the experimental observations discussed in the previous sections. Highest occupied natural orbital (HONO) and lowest unoccupied natural orbital (LUNO) density plots are shown in Figure 6a,b. In both plots, the orbital density is largely delocalized over the

DOI: 10.1021/jacs.6b07882
J. Am. Chem. Soc. 2016, 138, 12648−12654

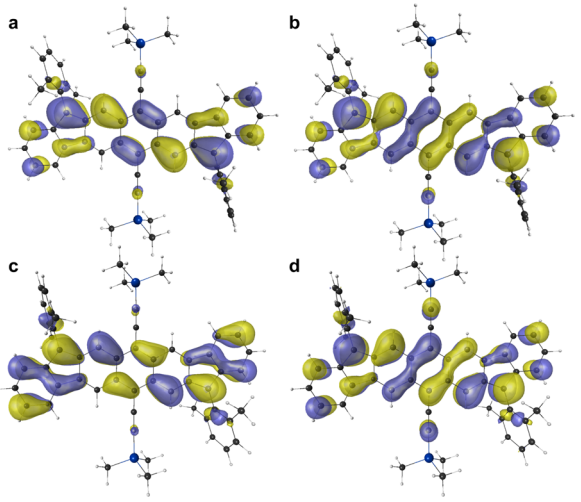

Figure 6. HONO (a) and LUNO (b) density plots of the neutral model **DIAn** in the singlet state at the LC-UBLYP/6-311+G** level of theory. SOMO density plots for the radical cation (c) and radical anion (d) doublet states at the LC-UBLYP/6-311+G** level of theory. Each plotted at 0.02 au isosurface value.

5-6-6-6-5 core of **DIAn**, with some density on the outer benzenoid rings. The SOMO density plots for $\mathbf{DIAn}^{\bullet+}$ and $\mathbf{DIAn}^{\bullet-}$ in their doublet states are depicted in Figure 6c,d. At first glance there is a strong resemblance between the neutral HONO density plot and radical cation SOMO density plot. Likewise, a similar relationship is evident between the neutral LUNO density plot and radical anion SOMO density plots. This is rationalized by recognizing that, in the first oxidation process, an electron is removed from the HONO, creating a singly occupied state of approximate orbital density and symmetry. Likewise, in the first reduction process, we observe a similar orbital symmetry and density between the monoanion SOMO and neutral LUNO. This is further supported by the small change in geometry from neutral **DIAn** to radical anion **1** upon reduction (Figure 5).

Electrostatic potential maps were calculated at the LC-UBLYP/6-311+G** on the **DIAn** model system and the two diionic states. For the neutral species we observe marginal charge on the core and substituents, as expected for a neutral species (Figure 7b). In the $\mathbf{DIAn}^{2-}$ model, regions of negative

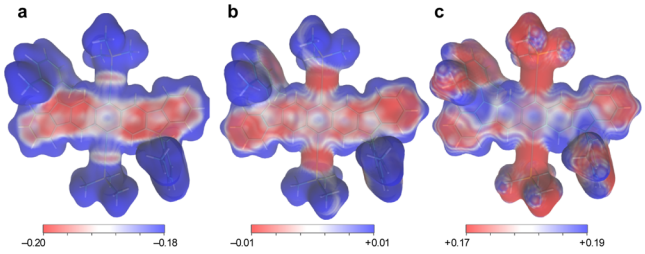

Figure 7. Electrostatic potential maps calculated at LC-UBLYP-(μ=0.33)/6-311+G** for the model **DIAn** in the dianionic (a), neutral (b), and dicationic states (c). Red (blue) regions represent more (less) negative charge for (a); negative (positive) charge for (b); and less (more) positive charge for (c).

charge (red) are localized near the five-membered ring and adjacent ring on the anthracene core (Figure 7a). The central benzenoid ring and ethynyl substituents show a distinct lack of charge. Moving to $\mathbf{DIAn}^{2+}$, an analogous distribution of charge is apparent with the five-membered rings containing the most electropositive regions (blue, Figure 7c). Along with the electrostatic potential maps, a Hirshfeld charge analysis (Supporting Information) indicates that charges in both diionic states are greatest on the apical carbon atoms connecting the outer benzenoid rings and the inner anthracene. This is in excellent agreement with the solid-state structure of **3**, as the K atoms are bonded in η^5- and η^6-coordination modes. An alternative explanation could be that these are also the most accessible sites on the **DIAn** core owing to the bulkiness of Si(i-Pr)$_3$ and Mes substituents. Nevertheless, the computational studies are in good agreement with experimental data and the redox processes outlined above.

CONCLUSIONS

We have shown that **DIAn** is a cyclopenta-fused PCH that can accept or donate electrons reversibly with charges primarily localized on the five-membered rings. As a result of the biradical character and the resonance relationship between quinoidal (acceptor) and aromatic (donor) structures in the ground state, **DIAn** is able to stabilize both negative and positive charges. Through spectroelectrochemical experiments, we identified low-energy absorptions (ca. 0.7 eV) in the monoradical states and assigned these transitions to HOMO → SOMO for $\mathbf{DIAn}^{\bullet-}$ and SOMO → LUMO for $\mathbf{DIAn}^{\bullet+}$ by TD-DFT methods. Raman spectroscopy in conjunction with in situ electrolysis indicated that the structures of radical cation/anion and dication/dianion states are quite similar. This translates to a minimal change in geometry upon polaronic-like formation, an attractive feature for organic electronic applications as large structural reorganization typically hampers electronic performance.[45] Investigation of the non-contact crown-ether potassium salts of $\mathbf{DIAn}^{\bullet-}$ and $\mathbf{DIAn}^{2-}$ through single-crystal X-ray diffraction provided a clear picture of the structural consequences of successive single-electron charging. Finally, a quantum chemical computational study supported our experimental results and detailed the localization of charge on the polycyclic core. From multiple experimental and spectroscopic techniques, we conclude that the cyclopenta-fused rings are the predominant sites of the rich redox chemistry observed in **DIAn**, in accord with the sites of highest odd-electron density in the ground state.[27] This study represents a unique case where the stability of a neutral open-shell compound allows for the thorough characterization and structural analysis across five redox states. Future work will focus on tuning the solid-state packing and device performance of the diindeno[b,i]anthracene system.

ASSOCIATED CONTENT

Supporting Information

The Supporting Information is available free of charge on the ACS Publications website at DOI: 10.1021/jacs.6b07882.

Experimental procedures, computational details and xyz coordinates, and copies of spectra (PDF)
Crystallographic data for **1** (CIF)
Crystallographic data for **2** (CIF)
Crystallographic data for **3** (CIF)

AUTHOR INFORMATION

Corresponding Authors

*mnaka@cheng.es.osaka-u.ac.jp
*mpetrukhina@albany.edu
*casado@uma.es
*haley@uoregon.edu

DOI: 10.1021/jacs.6b07882
J. Am. Chem. Soc. 2016, 138, 12648−12654

Notes

The authors declare no competing financial interest.

■ ACKNOWLEDGMENTS

This work was supported by the U.S. National Science Foundation (CHE-1301485 and CHE-1565780 to M.M.H., CHE-1212441 to M.A.P.), by the Spanish Government, MINECO (CTQ2015-69391-P and CTQ2015-67755-C2-1-R), and by the Japan Society for the Promotion of Science (JSPS), KAKENHI Grant Numbers JP15J04949, JP25248007, JP24109002, JP15H00999, and JP26107004. We thank Profs. V. García Baonza and M. Taravillo for use of the pressure cells in this study. We thank the Center for Research Support at the University of Málaga (SCAI) for access to the vibrational spectroscopic facilities. We also acknowledge the National Science Foundation for instrumentation grants (CHE-1337594 to M.A.P. and CHE-1427987 to M.M.H.).

■ REFERENCES

(1) Müllen, K. *Chem. Rev.* **1984**, *84*, 603−684.
(2) Benshafrut, R.; Shabtai, E.; Rabinovitz, M.; Scott, L. T. *Eur. J. Org. Chem.* **2000**, *2000*, 1091−1106.
(3) Bock, H.; Gharagozloo-Hubmann, K.; Sievert, M.; Prisner, T.; Havlas, Z. *Nature* **2000**, *404*, 267−269.
(4) Zabula, A. V.; Filatov, A. S.; Spisak, S. N.; Rogachev, A. Yu.; Petrukhina, M. A. *Science* **2011**, *333*, 1008−1011.
(5) Sternfeld, T.; Rabinovitz, M. In *Carbon-Rich Compounds: From Molecules to Materials*; Haley, M. M., Tykwinski, R. R., Eds.; Wiley-VCH: Weinheim, Germany, 2006; pp 566−624.
(6) *Organic Redox Systems: Synthesis, Properties and Applications*; Nishinaga, T., Ed.; Wiley: Hoboken, NJ, 2016.
(7) Huskinson, B.; Marshak, M. P.; Suh, C.; Er, S.; Gerhardt, M. R.; Galvin, C. J.; Chen, X.; Aspuru-Guzik, A.; Gordon, R. G.; Aziz, M. J. *Nature* **2014**, *505*, 195−198.
(8) Larcher, D.; Tarascon, J.-M. *Nat. Chem.* **2015**, *7*, 19−29.
(9) Abe, M. *Chem. Rev.* **2013**, *113*, 7011−7088.
(10) Zeng, Z.; Shi, X.; Chi, C.; López Navarrete, J. T.; Casado, J.; Wu, J. *Chem. Soc. Rev.* **2015**, *44*, 6578−6596.
(11) Kubo, T. *Chem. Lett.* **2015**, *44*, 111−122.
(12) Sun, Z.; Zeng, Z.; Wu, J. *Acc. Chem. Res.* **2014**, *47*, 2582−2591.
(13) Sun, Z.; Ye, Q.; Chi, C.; Wu, J. *Chem. Soc. Rev.* **2012**, *41*, 7857−7889.
(14) Nakano, M.; Kishi, R.; Nitta, T.; Kubo, T.; Nakasuji, K.; Kamada, K.; Ohta, K.; Champagne, B.; Botek, E.; Yamaguchi, K. *J. Phys. Chem. A* **2005**, *109*, 885−891.
(15) Motomura, S.; Nakano, M.; Fukui, H.; Yoneda, K.; Kubo, T.; Carion, R.; Champagne, B. *Phys. Chem. Chem. Phys.* **2011**, *13*, 20575−20583.
(16) Anthony, J. E. *Chem. Rev.* **2006**, *106*, 5028−5048.
(17) Anthony, J. E.; Facchetti, A.; Heeney, M.; Marder, S. R.; Zhan, X. *Adv. Mater.* **2010**, *22*, 3876−3892.
(18) Zhou, K.; Dong, H.; Zhang, H.-L.; Hu, W. *Phys. Chem. Chem. Phys.* **2014**, *16*, 22448−22457.
(19) Zhao, Y.; Guo, Y.; Liu, Y. *Adv. Mater.* **2013**, *25*, 5372−5391.
(20) Janoschka, T.; Hager, M. D.; Schubert, U. S. *Adv. Mater.* **2012**, *24*, 6397−6409.
(21) Morita, Y.; Nishida, S.; Murata, T.; Moriguchi, M.; Ueda, A.; Satoh, M.; Arifuku, K.; Sato, K.; Takui, T. *Nat. Mater.* **2011**, *10*, 947−951.
(22) Lee, J.; Lee, E.; Kim, S.; Bang, G. S.; Shultz, D. A.; Schmidt, R. D.; Forbes, M. D. E.; Lee, H. *Angew. Chem., Int. Ed.* **2011**, *50*, 4414−4418.
(23) Barnes, J. C.; Fahrenbach, A. C.; Cao, D.; Dyar, S. M.; Frasconi, M.; Giesener, M. A.; Benitez, D.; Tkatchouk, E.; Chernyashevskyy, O.; Shin, W. H.; Li, H.; Sampath, S.; Stern, C. L.; Sarjeant, A. A.; Hartlieb, K. J.; Liu, Z.; Carmieli, R.; Botros, Y. Y.; Choi, J. W.; Slawin, A. M. Z.; Ketterson, J. B.; Wasielewski, M. R.; Goddard, W. A.; Stoddart, J. F. *Science* **2013**, *339*, 429−433.
(24) Chase, D. T.; Fix, A. G.; Kang, S. J.; Rose, B. D.; Weber, C. D.; Zhong, Y.; Zakharov, L. N.; Lonergan, M. C.; Nuckolls, C.; Haley, M. M. *J. Am. Chem. Soc.* **2012**, *134*, 10349−10352.
(25) Koike, H.; Chikamatsu, M.; Azumi, R.; Tsutsumi, J.; Ogawa, K.; Yamane, W.; Nishiuchi, T.; Kubo, T.; Hasegawa, T.; Kanai, K. *Adv. Funct. Mater.* **2016**, *26*, 277−283.
(26) Kubo, T.; Shimizu, A.; Sakamoto, M.; Uruichi, M.; Yakushi, K.; Nakano, M.; Shiomi, D.; Sato, K.; Takui, T.; Morita, Y.; Nakasuji, K. *Angew. Chem., Int. Ed.* **2005**, *44*, 6564−6568.
(27) Rudebusch, G. E.; Zafra, J. L.; Jorner, K.; Fukuda, K.; Marshall, J. L.; Arrechea-Marcos, I.; Espejo, G. L.; Ortiz, R. P.; Gómez-García, C. J.; Zakharov, L. N.; Nakano, M.; Ottosson, H.; Casado, J.; Haley, M. M. *Nat. Chem.* **2016**, *8*, 753−759.
(28) Yamaguchi, K. In *Self-Consistent Field: Theory and Applications*; Carbo, R., Klobukowski, M., Eds.; Elsevier: Amsterdam, The Netherlands, 1990; pp 727−828.
(29) Shimizu, A.; Hirao, Y.; Matsumoto, K.; Kurata, H.; Kubo, T.; Uruichi, M.; Yakushi, K. *Chem. Commun.* **2012**, *48*, 5629−5631.
(30) Dong, S.; Herng, T. S.; Gopalakrishna, T. Y.; Phan, H.; Lim, Z. L.; Hu, P.; Webster, R. D.; Ding, J.; Chi, C. *Angew. Chem., Int. Ed.* **2016**, *55*, 9316−9320.
(31) Huang, R.; Phan, H.; Herng, T. S.; Hu, P.; Zeng, W.; Dong, S.-Q.; Das, S.; Shen, Y.; Ding, J.; Casanova, D.; Wu, J. *J. Am. Chem. Soc.* **2016**, *138*, 10323−10330.
(32) Chase, D. T.; Fix, A. G.; Rose, B. D.; Weber, C. D.; Nobusue, S.; Stockwell, C. E.; Zakharov, L. N.; Lonergan, M. C.; Haley, M. M. *Angew. Chem., Int. Ed.* **2011**, *50*, 11103−11106.
(33) Rose, B. D.; Vonnegut, C. L.; Zakharov, L. N.; Haley, M. M. *Org. Lett.* **2012**, *14*, 2426−2429.
(34) Young, B. S.; Chase, D. T.; Marshall, J. L.; Vonnegut, C. L.; Zakharov, L. N.; Haley, M. M. *Chem. Sci.* **2014**, *5*, 1008−1014.
(35) Rudebusch, G. E.; Fix, A. G.; Henthorn, H. A.; Vonnegut, C. L.; Zakharov, L. N.; Haley, M. M. *Chem. Sci.* **2014**, *5*, 3627−3633.
(36) Haley, M. M. *Chem. Rec.* **2015**, *15*, 1140−1143.
(37) Marshall, J. L.; Uchida, K.; Frederickson, C. K.; Schütt, C.; Zeidell, A. M.; Goetz, K. P.; Finn, T. W.; Jarolimek, K.; Zakharov, L. N.; Risko, C.; Herges, R.; Jurchescu, O. D.; Haley, M. M. *Chem. Sci.* **2016**, *7*, 5547−5558.
(38) Mondal, R.; Tönshoff, C.; Khon, D.; Neckers, D. C.; Bettinger, H. F. *J. Am. Chem. Soc.* **2009**, *131*, 14281−14289.
(39) Cataldo, F.; Iglesias-Groth, S.; Manchado, A. *Spectrochim. Acta, Part A* **2010**, *77*, 998−1004.
(40) Ohashi, K.; Kubo, T.; Masui, T.; Yamamoto, K.; Nakasuji, K.; Takui, T.; Kai, Y.; Murata, I. *J. Am. Chem. Soc.* **1998**, *120*, 2018−2027.
(41) We unfortunately were not able to obtain diffraction quality crystals of the radical cation and dication of **DIAn**, prepared by either chemical oxidation or electrocrystallization.
(42) Zabula, A. V.; Spisak, S. N.; Filatov, A. S.; Grigoryants, V. M.; Petrukhina, M. A. *Chem. - Eur. J.* **2012**, *18*, 6476−6484.
(43) Casado, J.; Miller, L. L.; Mann, K. R.; Pappenfus, T. M.; Higuchi, H.; Ortí, E.; Milián, B.; Pou-AméRigo, R.; Hernández, V.; López Navarrete, J. T. *J. Am. Chem. Soc.* **2002**, *124*, 12380−12388.
(44) Rose, B. D.; Sumner, N. J.; Filatov, A. S.; Peters, S. J.; Zakharov, L. N.; Petrukhina, M. A.; Haley, M. M. *J. Am. Chem. Soc.* **2014**, *136*, 9181−9189.
(45) Yavuz, I.; Martin, B. N.; Park, J.; Houk, K. N. *J. Am. Chem. Soc.* **2015**, *137*, 2856−2866.

DOI: 10.1021/jacs.6b07882
J. Am. Chem. Soc. 2016, 138, 12648−12654